The donor star radial velocity curve in the cataclysmic variable GY Cnc confirms white dwarf eclipse modelling mass

S. P. Littlefair [1]*, Pablo Rodríguez-Gil [2,3] T. R. Marsh [4], S. G. Parsons [1] and V. S. Dhillon [1,3]

[1]*Department of Physics and Astronomy, University of Sheffield, Sheffield S3 7RH, UK*
[2]*Instituto de Astrofísica de Canarias, E-38205 La Laguna, Tenerife, Spain*
[3]*Departamento de Astrofísica, Universidad de La Laguna, E-38206 La Laguna, Tenerife, Spain*
[4]*Department of Physics, University of Warwick, Coventry CV4 7AL, UK*

ABSTRACT

A large number of white dwarf and donor masses in cataclysmic variables have been found via modelling the primary eclipse, a method that relies on untested assumptions. Recent measurements of the mass of the white dwarf in the cataclysmic variable GY Cnc, obtained via modelling its ultraviolet spectrum, conflict with the mass obtained via modelling the eclipse light curve. Here we measure the radial velocity of the absorption lines from the donor star in GY Cnc to be $K_{\rm abs} = 280 \pm 2$ km s^{-1}, in excellent agreement with the prediction based on the masses derived from modelling the eclipse light curve. It is possible that the white dwarf mass derived from the ultraviolet spectrum of GY Cnc is affected by the difficulty of disentangling the white dwarf spectrum from the accretion disc spectrum.

Key words: binaries: eclipsing – stars: dwarf novae – stars: evolution – novae, cataclysmic variables – white dwarfs.

1 INTRODUCTION

Cataclysmic variables (CVs) are interacting binaries in which a white dwarf accretes material from a low-mass companion (the donor star). CVs are a valuable test-bed for binary evolution, since their long-term evolution is driven by angular momentum loss from the binary. For an in-depth review of the evolution of CVs, see Knigge, Baraffe & Patterson (2011).

The current predictions of CV evolution (e.g. Kolb 1993; Howell, Nelson & Rappaport 2001) are in tension with the high average white dwarf masses in CVs (Zorotovic, Schreiber & Gänsicke 2011) and the scarcity of CVs that have evolved past the period minimum (Pala et al. 2020). There are also issues with the generally accepted explanation for the period gap (Andronov, Pinsonneault & Sills 2003; Garraffo et al. 2018; El-Badry et al. 2022). Solutions to many of these problems may be found by invoking additional sources of angular momentum loss from the binary. For example, Schreiber, Zorotovic & Wijnen (2016) suggest that additional angular momentum loss caused by binary interactions with novae ejecta could solve many of the outstanding issues with CV evolution, and theoretical models of novae outflows seem to support such a mechanism (Shen & Quataert 2022).

The cause and magnitude of angular momentum loss from CVs is therefore quite uncertain, and likely to be key to understanding their evolution. This makes observational constraints important. The best observational constraints on the angular momentum loss rates come from measurements of the *long term* mass transfer rate, $\dot{M}$, provided these measures average over longer time-scales than any possible short term fluctuations (Knigge, Baraffe & Patterson 2011). Two methods satisfy this requirement: White dwarf effective

temperatures measure the mass transfer rate averaged over $\sim 10^4$ yr (Townsley & Bildsten 2003; Knigge, Baraffe & Patterson 2011; Pala et al. 2022). Donor star radii measure an average of the mass transfer rate over $\sim 10^8$ yr (Knigge, Baraffe & Patterson 2011), making them potentially the best test of secular mass transfer rates.

Precise measures of the masses and radii of the donors and white dwarfs in CVs are difficult to obtain. This is because the accretion disc often outshines the donor star and white dwarf, so CVs very rarely present as double-lined eclipsing binaries. In some cases, the white dwarf is visible in the ultraviolet, and spectroscopic modelling can yield the white dwarf mass and temperature (e.g. Godon & Sion 2022; Pala et al. 2022). However, the majority of precise component masses for CVs arise from modelling of the shape of the primary eclipse, hereafter called the *photometric eclipse method* (e.g. Feline et al. 2005; Littlefair et al. 2006; Savoury et al. 2011; McAllister et al. 2019).

Masses derived from the photometric eclipse method have small statistical errors, and have been independently confirmed in a few systems where it is also possible to measure radial velocities via spectroscopy (Tulloch, Rodríguez-Gil & Dhillon 2009; Copperwheat et al. 2012; Savoury et al. 2012). However, they are underpinned by untested assumptions. In particular, to infer the white dwarf radius from the ingress/egress duration, it is assumed that the whole white dwarf is visible and that the white dwarf surface brightness is uniform (apart from limb darkening). There are good reasons to suspect this is not true in all CVs. First, the presence of gas between the observer and white dwarf surface is well established. This gas is revealed by the so-called 'iron curtain' – a forest of absorption lines in the blue and ultraviolet spectra of CVs (Horne et al. 1994). It is quite possible that absorption from the iron curtain could mean that we do not see the whole white dwarf surface. In addition, a boundary layer exists near the white dwarf surface, where the rapidly rotating

* E-mail: s.littlefair@shef.ac.uk

disc material transforms kinetic energy into heat and radiation. It is possible that the 'white dwarf ingress' seen during eclipse is in fact dominated by the boundary layer itself and not the white dwarf surface. Spark & O'Donoghue (2015) present high-cadence light curves of white dwarf eclipses that appear to show departures from the expected shape of a limb-darkened white dwarf. These departures may be the result of random flickering, but they may also represent a breakdown in the assumptions underpinning the photometric eclipse method.

Godon & Sion (2022) present a recent independent test of photometrically derived white dwarf masses. Using *Gaia* eDR3 parallaxes, and archival *Hubble Space Telescope* ultraviolet spectroscopy, they model the white dwarf and the iron curtain simultaneously and derive a white dwarf mass directly from the ultraviolet spectrum. Five of the systems modelled have independent masses derived from the eclipse light curve, and for four of the five systems excellent agreement is found. However, the fifth system, GY Cnc (Gänsicke et al. 2000), is discrepant. Godon & Sion found a white dwarf mass of $M_1 = 0.57 \pm 0.05\,M_\odot$, compared to $M_1 = 0.88 \pm 0.02\,M_\odot$ obtained from modelling the eclipse light curve (McAllister et al. 2019), and they also found that modelling GY Cnc required a significant iron curtain, with a hydrogen column density of $5 \times 10^{21}\,cm^{-2}$. This raises the possibility that the masses in GY Cnc derived from eclipse modelling are incorrect and therefore brings into question all masses derived via eclipse modelling that do not have independent confirmation.

In this paper, we present archival spectroscopy of GY Cnc that reveals the orbital motion of the donor star. We measure the velocity of the donor star's absorption lines, and determine if it is consistent with the system parameters measured by McAllister et al. (2019) from the eclipse light curve.

2 OBSERVATIONS AND DATA REDUCTION

GY Cnc was observed on the night of 2006 April 14 using ISIS on the 4.2-m William Herschel Telescope (WHT) at La Palma, Spain, as part of programme NL/2006A/5 (PI: Ham). Note that in this study, we only analyse data from the red arm of ISIS: the R316R grating used with a 1-arcsec slit and a central wavelength of 6304 Å. The detector was binned by a factor of 2 in the spatial and spectral directions, giving an unvignetted wavelength coverage of 5400–7950 Å and a resolution of approximately 3.8 Å. The slit was rotated to a sky position angle of 101° to include the spectrum of Gaia DR3 635520611367973120 on the slit, to help measure the telluric contamination of the GY Cnc spectra. A total of 219 exposures with an exposure time of 50 s were taken, but the first 20 and the last 14 spectra were affected by clouds and were discarded. The resulting time series covers from UT 20:30 to 00:30. Frequent CuNe + CuAr arcs were taken during the night to ensure accurate wavelength calibration.

The raw data were reduced, and spectra of both objects extracted using the PYTHON package ASPIRED (Lam et al. 2023). Raw images were de-biased and corrected for uneven slit illumination and pixel response non-uniformity using observations of a tungsten lamp. The spatial positions of the spectra were traced with a third order polynomial and spectra were extracted using an aperture of width 12 pixels and the optimal extraction method of Horne (1986). The sky was subtracted using a first-order polynomial fit to pixel values in a pair of strips of width 6 pixels, separated by 5 pixels from the edges of the object aperture.

Wavelength calibration for each spectrum was carried out using the arc spectrum taken nearest in time. A second-order polynomial was
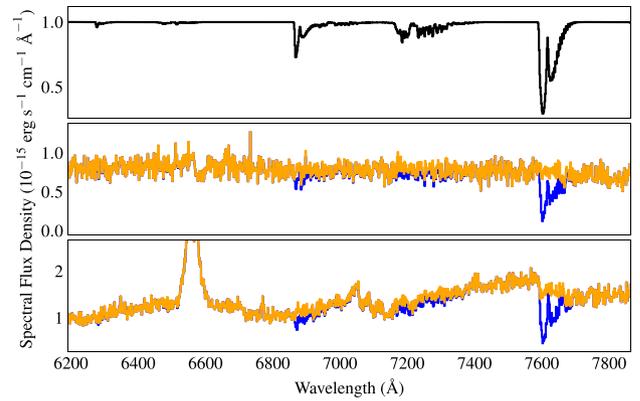
Figure 1. Telluric correction of spectra. Top: The best-fitting theoretical telluric spectrum found by fitting the LBLRTM to the spectrum of Gaia DR3 635520611367973120. Middle: an individual spectrum of Gaia DR3 635520611367973120 (blue) and the same spectrum after correcting with the theoretical telluric spectrum above (orange). Bottom: the spectrum of GY Cnc, zoomed in to focus on the donor star features before (blue) and after (orange) telluric correction.

used to fit the relation between pixel number and wavelength with root-mean-square residuals of the order of 0.4 Å, which is less than a single pixel. The spectra were flux calibrated using observations of the DA7 white dwarf Gaia DR3 4452521234885949184.

Telluric correction was carried out using the PYTHON package TELFIT (Gullikson, Dodson-Robinson & Kraus 2014). TELFIT calculates a theoretical telluric spectrum using the line by line radiative transfer model (LBLRTM; Clough et al. 2005), and optimizes the atmospheric parameters to find the telluric spectrum that best matches the observed spectrum. We calculated the telluric spectrum using the relatively featureless spectrum of Gaia DR3 635520611367973120 (K4V), and used this theoretical telluric spectrum to correct the spectra of GY Cnc. An example is given in Fig. 1.

3 RESULTS

Analysis of the reduced spectra was carried out using MOLLY.[1] All spectra were corrected for the velocity shift of the observer with respect to the Solar System Barycenter and binned onto an identical wavelength scale with bins uniformly spaced in velocity units. Spectra were normalized by dividing by a second order polynomial fit, and cosmic rays were iteratively removed from the spectra by clipping pixels whose values lay more than 5σ away from the mean value of the equivalent pixels in the entire time series. The average spectrum of GY Cnc in the rest frame of the donor star (using the radial velocity found in Section 3.2) is shown in Fig. 2.

Because the spectrum of GY Cnc shows strong absorption features from the donor star, we can use them to measure its radial velocity and test which of the two claimed white dwarf masses for GY Cnc is correct.

3.1 Trailed spectra

Fig. 3 shows the trailed spectra of GY Cnc, where each spectrum is represented as a row in the image, and the brightness of the image

---

[1]MOLLY was written by T. R. Marsh and is available at http://www. warwick. ac.uk/go/trmarsh/software
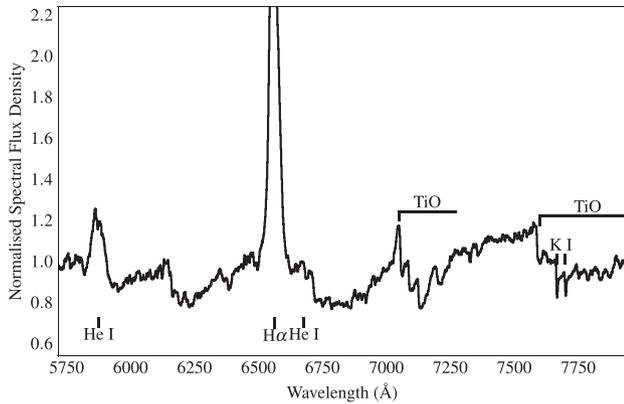
Figure 2. Average spectrum of GY Cnc cropped to focus on the donor star features. The spectrum is presented in the rest frame of the donor star, using the radial velocity found in Section 3.2. Absorption bands of TiO and the K I doublet from the donor star are visible along with strong, double-peaked emission lines from the disc. The continuum shape has been removed with a second order polynomial fit.

represents the spectral flux density. Orbital phases for each spectrum were calculated using the ephemeris of McAllister et al. (2019). The trailed spectra reveal that the TiO bandheads and the K I absorption lines trace the motion of the donor star, but also show that our telluric correction is not perfect. Residual telluric lines form vertical streaks in the trailed spectra and the residuals from the strong telluric region contaminate the TiO bandhead at 7600 Å. However, the TiO bandhead at 7050 Å and the K I doublet at 7680 Å remain largely free of contamination from telluric features, and should therefore be suitable for determining the radial velocity of the donor star. Indeed, visual inspection of the motion of the K I lines in Fig. 3 appears to support a radial velocity amplitude for the donor star of $\simeq 280$ km s^{-1}, larger than the prediction assuming the white dwarf mass of Godon & Sion (2022) and comparable to the value predicted using the white dwarf mass of McAllister et al. (2019) (see Section 4 for more details).

3.2 Radial velocity curve of the donor star

We derive the amplitude of the radial velocity curve of the donor star's absorption lines, K_{abs}, by cross correlating the normalized spectra of GY Cnc against a solar-metallicity M3 V spectral template from Kesseli et al. (2017). These templates are produced from Sloan Digital Sky Survey (SDSS) spectroscopy with a resolution of $R \approx 2000$, which is well matched to our data. Templates with spectral types from M1 V to M5 V (see Section 3.3) were trialled, with no significant difference in the results.

The spectra were first cropped to exclude data outside the range 6750–7900 Å, and normalized by dividing by their means. Following this, a first order polynomial fit was subtracted from both spectrum and template, and both spectra were resampled onto the same wavelength scale, which is uniformly spaced in log-wavelength. Prior to cross-correlation, both spectra were apodized by multiplying by a cosine function that is restricted to the first and last 5 per cent of the spectrum; this reduces the impact of edge effects. Cross-correlation was performed on the flux data of the two spectra, weighted by the uncertainties on the spectrum of GY Cnc. From the cross-correlation of GY Cnc and template, radial velocities and their uncertainties were found by fitting a parabola to the three points nearest the peak of the cross-correlation. Radial velocities are shown in Fig. 4.

Orbital phases for each spectrum were calculated using the ephemeris of McAllister et al. (2019), and a sinusoid was fitted to the radial velocities:

$$V(\phi) = V_{sys} + K_{abs} \sin[2\pi(\phi + \phi_0)] , \qquad (1)$$

with ϕ the orbital phase and V_{sys} the systemic velocity. ϕ_0 is an offset in phase that allows for the possibility that the radial velocity of the donor is not zero at mid-eclipse. The best-fitting solution has $K_{abs} = 280 \pm 2$ km s^{-1}, $\phi_0 = -0.02 \pm 0.02$, and $V_{sys} = 3 \pm 2$ km s^{-1} and is shown in Fig. 4. The residuals to our fit indicate systematic deviations from a pure sinusoid that may reveal the effects of irradiation on the absorption line strength, or the effects of starspots. However, the solution has a reduced chi-squared of $\chi^2_\nu = 0.54$, indicating that the uncertainties on the radial velocities are slightly overestimated. These deviations are therefore unlikely to significantly affect our estimate of K_{abs}.

3.3 Donor star spectral type

Using $K_{abs} = 280$ km s^{-1}, we created an average spectrum of GY Cnc in the rest frame of the donor star, and compared to the solar-metallicity library templates of Kesseli et al. (2017). The templates and GY Cnc spectra were normalized using a first order polynomial fit and resampled onto the same wavelength scale. For each template, we added a range of constant values to simulate contamination by accretion disc light, and re-normalized. The best-fitting template and contamination levels were found by subtracting the template from the GY Cnc spectrum to create a residual spectrum. We then calculate the χ^2 of the residual spectrum, and a smoothed version of itself (Gaussian smoothing, $\sigma = 10$ pixels). This reduces the impact of continuum shape on the figure of merit, which is dominated by the strengths of the TiO and K I absorption features. A comparison between GY Cnc and the best-fitting spectrum at each spectral type is shown in Fig. 5. The best-fitting template has a spectral type of M5 V. This is slightly later than suggested by the semi-empirical donor star sequence of Knigge, Baraffe & Patterson (2011), which predicts a spectral type of M3 V at the orbital period of GY Cnc. Based on visual inspection, Thorstensen (2000) find a spectral type of M3 V. The M3 V template is a much poorer fit to our data ($\chi^2 = 2932$, 568 D.O.F) than the M5 V template ($\chi^2 = 2578$, 568 D.O.F). This is largely driven by the strength of the TiO bandhead at 760 nm.

### 3.4 Radial velocity of the emission line wings

It is not possible to directly measure the radial velocity of the white dwarf, as no spectral features are visible. Historically, mass determinations in CVs have attempted to estimate the white dwarf radial velocity via the motion of the emission line wings. The motion of the line wings can be determined using the method of Schneider & Young (1980). An emission line profile is convolved with a double-Gaussian profile, each Gaussian having the same width but opposite amplitudes. When the Gaussians are centred on the emission line, the convolution vanishes, determining the radial velocity. At large separations of the Gaussians, one measures the velocity of the emission line wings, formed in the high-velocity gas near the white dwarf. It is hoped that the motion of this gas traces the white dwarf itself, although whether this is true is far from certain.

We measure the velocities of the Hα line wings using this approach. For a given separation of the Gaussians, we fit a sinusoidal radial velocity curve:

$$V(\phi) = V_{sys} - K_{em} \sin[2\pi(\phi + \phi_0)] . \qquad (2)$$
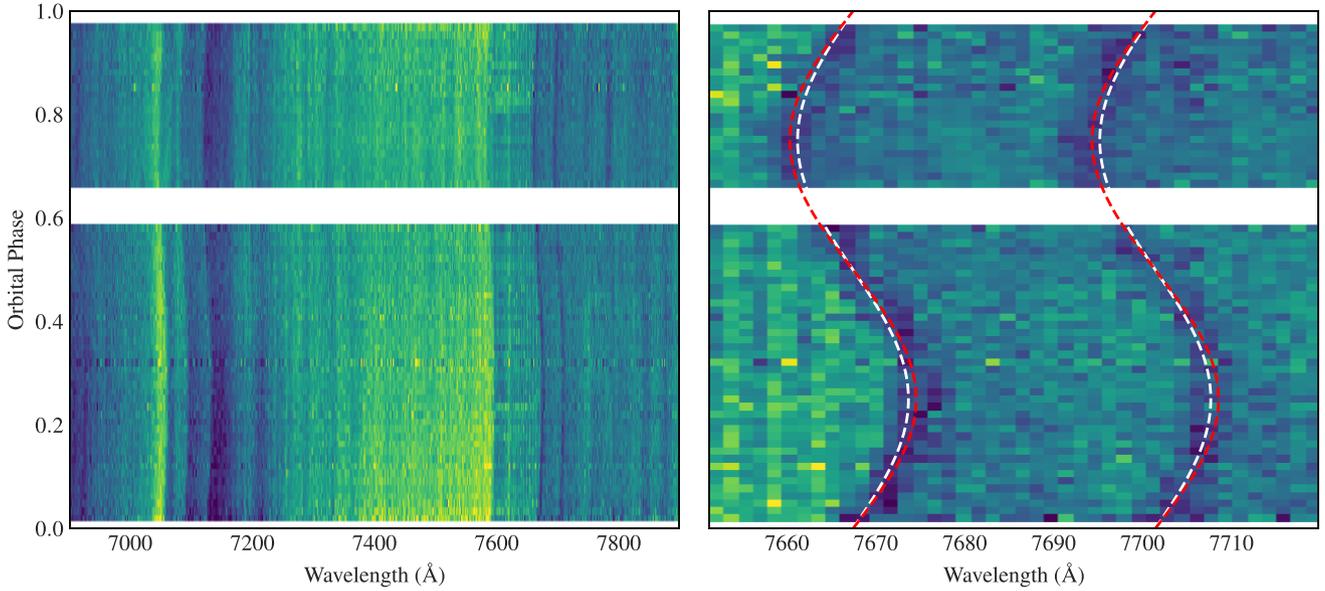
Figure 3. The normalized trailed spectra of GY Cnc, focusing on the donor star features redwards of 6900 Å. The left panel shows the strong TiO bandheads at 7050 and 7600 Å, which clearly trace the donor star's radial velocity. Vertical stripes, and the noisy region around 7600 Å represent imperfect subtraction of telluric features. The right-hand panel shows a zoomed region around the K I doublet at 7665/7699 Å. Superimposed are dashed lines showing two potential solutions for the radial velocity of the donor star, one with 244 km s^{-1} (white) and one with 278 km s^{-1} amplitude (red). These two velocities represent the estimated donor star velocity assuming the white dwarf masses of Godon & Sion ([2022](#)) and McAllister et al. ([2019](#)), respectively.
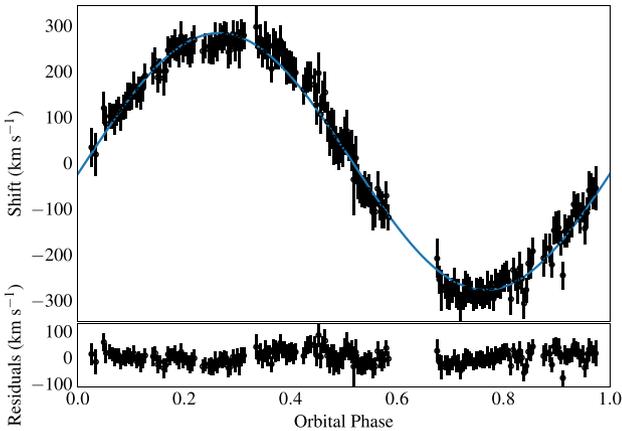
Figure 4. Radial velocities for the absorption features in GY Cnc, measured via cross-correlation and plotted as a function of orbital phase. Points with uncertainties show the radial velocity measurements. The blue line shows the best-fitting sinusoid.

A diagnostic diagram, showing the fit parameters of this curve versus the Gaussian separation is shown in Fig. [6](#). With a Gaussian separation of 3000 km s^{-1} we find $K_{em} = 129 \pm 3$ km s^{-1}, $\phi_0 = -0.05 \pm 0.06$, and $V_{sys} = -76 \pm 3$ km s^{-1}. These uncertainties do not include the systematic uncertainty arising from choosing an appropriate Gaussian separation, which can change the measured velocities by tens of km s^{-1}.

Whilst we strongly caution against interpreting K_{em} as the velocity of the white dwarf, we note that our value is not too far away from the value measured by Thorstensen ([2000](#)) of $K_{em} = 116 \pm 5$ km s^{-1} from the same line, and is in agreement with the predicted white dwarf velocity $K_{wd} = 125 \pm 4$ km s^{-1} of McAllister et al. ([2019](#)).

4 DISCUSSION

Based on modelling of the eclipse light curve, and a theoretical white dwarf mass–radius relation, McAllister et al. ([2019](#)) predict a donor star radial velocity amplitude of $K_2 = 278 \pm 2$ km s^{-1} for GY Cnc. This compares very well with the velocity we measure for the absorption lines, $K_{abs} = 280 \pm 2$ km s^{-1}, and indicates a preference for the system parameters of McAllister et al. ([2019](#)) over those of Godon & Sion ([2022](#)). However, care must be taken, since the centre of light of the donor absorption lines does not necessarily correspond to its centre of mass (e.g. Watson et al. [2003](#)). In particular, irradiation from the white dwarf can strengthen or weaken absorption lines near the L1 point, so that $K_{abs} \neq K_2$. Non-uniform light distribution on the donor star can be detected in the radial velocity curves as a departure from a sinusoidal fit. Our data lack the precision to see this effect and thus we cannot quantify any difference between K_{abs} and K_2.

In the case of GY Cnc, the spectral type of M5 V means that the TiO bandheads will weaken with increasing temperature. Thus, these features are expected to be weaker near the L1 point if this region is significantly hotter (see Fig. [5](#)). Therefore, it is reasonable to assume that in GY Cnc the centre of light will be shifted towards the back half of the donor star, implying $K_{abs} \geq K_2$. Since higher values of K_2 correspond to larger white dwarf masses, we are confident that the white dwarf mass of McAllister et al. ([2019](#)) should be preferred. We therefore asked ourselves if it is possible to use additional constraints to *rule out* the white dwarf mass of Godon & Sion ([2022](#)).

A detailed study of the donor absorption lines and radial velocity of the emission line wings in GY Cnc was carried out by Thorstensen ([2000](#)). Their measured $K_{abs} = 297 \pm 15$ km s^{-1} agrees with our value, within the uncertainties. To derive the white dwarf mass from their data the author assumed the wings of the emission lines trace the velocity of the white dwarf, and applied 'a frank guess' for the correction from K_{abs} to K_2. The result is a white dwarf mass of $M_1 = 0.82 \pm 0.14\,M_\odot$, which favours the higher white dwarf mass of
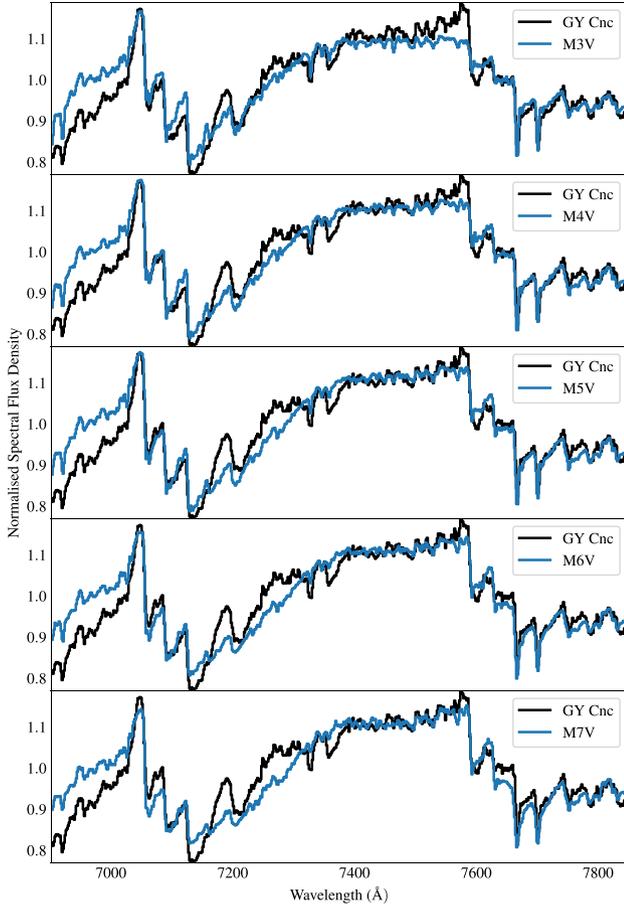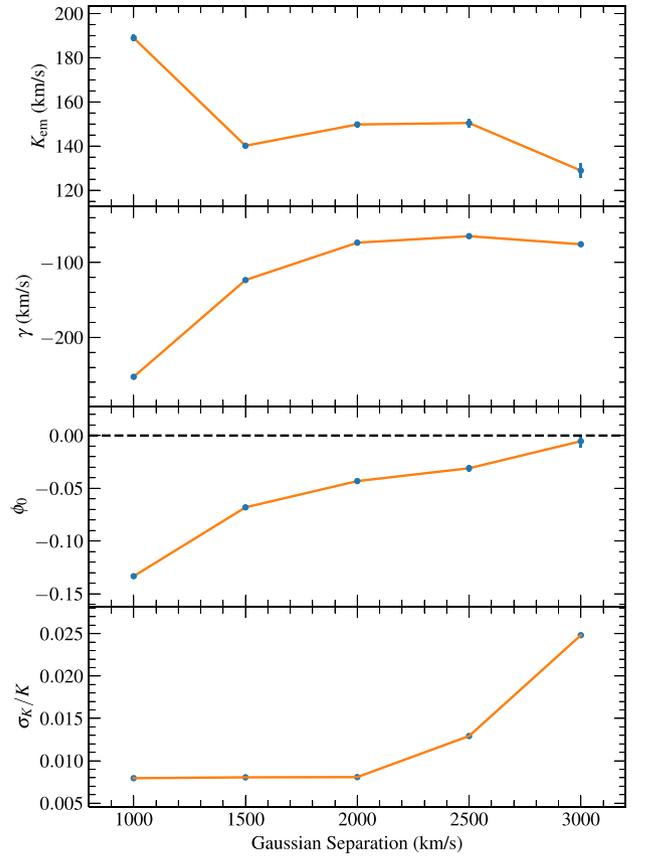
Figure 5. Comparison of the spectrum of GY Cnc to M-dwarf template spectra. The spectrum of GY Cnc in the rest frame of the donor star is shown in black, and template spectra are shown in blue. Spectra were normalized by dividing by the overall mean flux. See the text for details.

Figure 6. Diagnostic diagram for the H α emission line.

McAllister et al. (2019), but is only marginally inconsistent (1.7σ) with the lower mass of Godon & Sion (2003). Without the correction to K_{abs}, Thorstensen (2000) find $M_1 = 0.99 \pm 0.12\,M_\odot$, which is inconsistent with the mass of Godon & Sion (2003).

The component masses of a CV can be derived without assuming the emission lines reveal the white dwarf's velocity using measurements of the donor star's absorption lines and the phase width of the white dwarf eclipse, $\Delta\phi_{1/2}$ (e.g. Smith, Dhillon & Marsh 1998). However, this requires measurement of the rotational broadening of the donor star's absorption lines, $V_{rot}\sin i$, and our spectra lack the resolution for this. For the system parameters in McAllister et al. (2019), we would expect $V_{rot}\sin i \approx 125$ km s^{-1}, which corresponds to a broadening of less than one resolution element. Since we cannot measure $V_{rot}\sin i$, we can either adopt $q = 0.448$ from the light-curve fitting (McAllister et al. 2019), or we can adopt $q = K_{em}/K_{abs} = 0.46$ from the spectroscopic data (we do not include errors due to the difficulty assigning systematic errors to K_{em}). Because the value of K_{em} can change markedly depending on the Gaussian separation used, and because it is far from certain that the gas in the inner disc traces the radial velocity of the white dwarf, we prefer not to use K_{em} to measure the system parameters if an alternative is available.

We will therefore proceed by adopting the most robust parameters from the light-curve fitting of McAllister et al. (2019), although we note that our conclusions do not change, whichever value we adopt.

Criticisms of the eclipse light-curve modelling method mostly focus on inferring the white dwarf radius, and hence mass, from the ingress and egress widths of the white dwarf eclipse. Constraints upon the mass ratio, q, are independent of this effect, as they come largely from the timing of the bright spot eclipse. We assume here that $\Delta\phi_{1/2}$ is also robust. In principle, the width of the white dwarf eclipse could be affected by the same phenomena that affect the ingress and egress duration. However, in GY Cnc, the ingress and egress are so short, that any possible effect is smaller than the formal uncertainties on $\Delta\phi_{1/2}$.

In McAllister et al. (2019), eclipse light-curve modelling was used to find $q = 0.448^{+0.014}_{-0.021}$ and $\Delta\phi_{1/2} = 0.064 \pm 0.002$. Since $\Delta\phi_{1/2}$ is a function only of q and the inclination i, this yields $i = 77^\circ.1^{+0.3^\circ}_{-0.2^\circ}$. The orbital period is $P = 0.175442399(6)$ d, with the number in brackets being the uncertainty in the last digit. Kepler's third law allows us to write

$$M_1 = \frac{K_2^3\,P(1+q)^2}{2\pi\,G\sin^3 i}\;. \qquad (3)$$

Adopting $K_2 = K_{abs} = 280 \pm 2$ km s^{-1}, we find $M_1 = 0.90 \pm 0.03\,M_\odot$. Unsurprisingly, this is in good agreement with $M_1 = 0.88 \pm 0.02\,M_\odot$ from McAllister et al. (2019) and the less precise measure by Thorstensen (2000) of $M_1 = 0.99 \pm 0.12\,M_\odot$. It is however, more than 5σ different from the Godon & Sion (2022) white dwarf mass of $0.57 \pm 0.05\,M_\odot$, derived through careful modelling of the ultraviolet spectrum of GY Cnc. We therefore conclude that the higher white dwarf mass is correct and recommend the adoption of the system parameters in McAllister et al. (2019) for GY Cnc.

5 CONCLUSIONS

Stellar masses in CVs derived from modelling the white dwarf eclipses rely on several assumptions. There is little evidence for most of these assumptions and it is important to keep that in mind when using masses derived in this manner. However, whenever masses derived from light-curve modelling have been checked independently, they have proved to be consistent (Tulloch, Rodríguez-Gil & Dhillon 2009; Copperwheat et al. 2012; Savoury et al. 2012). GY Cnc was the only system for which Godon & Sion (2022) found a discrepancy between the white dwarf masses obtained from the eclipse light curve and ultraviolet spectroscopy. We show here that the white dwarf mass derived from the eclipse light curve is the correct one.

Therefore, we conclude that masses in CVs obtained via eclipse light-curve modelling are generally reliable. It is beyond the scope of this paper to establish why the analysis of the ultraviolet spectrum by Godon & Sion (2022) found an anomalously low white dwarf mass. However, we can speculate that it is related to the difficulty of analysing the white dwarf spectrum in the presence of contamination from the accretion disc, boundary layer, and iron curtain.

Whilst it is possible that applying eclipse light-curve modelling to any single system could produce incorrect masses due to the breakdown of the assumptions given in the introduction, there remains no known example where this has actually occurred. Thus, we recommend caution when drawing conclusions from the parameters of a single system, but believe that conclusions drawn from the wider population or the distribution of component masses are robust.

ACKNOWLEDGEMENTS

DATA AVAILABILITY

The data underlying this article will be shared on reasonable request to the corresponding author.

REFERENCES

Andronov N., Pinsonneault M., Sills A., 2003, ApJ, 582, 358
Clough S. A., Shephard M. W., Mlawer E. J., Delamere J. S., Iacono M. J., Cady-Pereira K., Boukabara S., Brown P. D., 2005, J. Quant. Spectrosc. Radiat. Transfer, 91, 233
Copperwheat C. M. et al., 2012, MNRAS, 421, 149
El-Badry K., Conroy C., Fuller J., Kiman R., van Roestel J., Rodriguez A. C., Burdge K. B., 2022, MNRAS, 517, 4916
Feline W. J., Dhillon V. S., Marsh T. R., Watson C. A., Littlefair S. P., 2005, MNRAS, 364, 1158
Gänsicke B. T., Fried R. E., Hagen H. J., Beuermann K., Engels D., Hessman F. V., Nogami D., Reinsch K., 2000, A&A, 356, L79
Garraffo C., Drake J. J., Alvarado-Gomez J. D., Moschou S. P., Cohen O., 2018, ApJ, 868, 60
Godon P., Sion E. M., 2003, ApJ, 586, 427
Godon P., Sion E. M., 2022, ApJ, 928, 26
Gullikson K., Dodson-Robinson S., Kraus A., 2014, AJ, 148, 53
Horne K., 1986, PASP, 98, 609
Horne K., Marsh T. R., Cheng F. H., Hubeny I., Lanz T., 1994, ApJ, 426, 294
Howell S. B., Nelson L. A., Rappaport S., 2001, ApJ, 550, 897
Kesseli A. Y., West A. A., Veyette M., Harrison B., Feldman D., Bochanski J. J., 2017, ApJS, 230, 16
Knigge C., Baraffe I., Patterson J., 2011, ApJS, 194, 28
Kolb U., 1993, A&A, 271, 149
Lam M. C., Smith R. J., Arcavi I., Steele I. A., Veitch-Michaelis J., Wyrzykowski L., 2023, AJ, 166, 13
Littlefair S. P., Dhillon V. S., Marsh T. R., Gänsicke B. T., Southworth J., Watson C. A., 2006, Science, 314, 1578
McAllister M. et al., 2019, MNRAS, 486, 5535
Pala A. F. et al., 2020, MNRAS, 494, 3799
Pala A. F. et al., 2022, MNRAS, 510, 6110
Savoury C. D. J. et al., 2011, MNRAS, 415, 2025
Savoury C. D. J., Littlefair S. P., Marsh T. R., Dhillon V. S., Parsons S. G., Copperwheat C. M., Steeghs D., 2012, MNRAS, 422, 469
Schneider D. P., Young P. J., 1980, ApJ, 238, 946
Schreiber M. R., Zorotovic M., Wijnen T. P. G., 2016, MNRAS, 455, L16
Shen K. J., Quataert E., 2022, ApJ, 938, 31
Smith D. A., Dhillon V. S., Marsh T. R., 1998, MNRAS, 296, 465
Spark M. K., O'Donoghue D., 2015, MNRAS, 449, 175
Thorstensen J. R., 2000, PASP, 112, 1269
Townsley D. M., Bildsten L., 2003, ApJ, 596, L227
Tulloch S. M., Rodríguez-Gil P., Dhillon V. S., 2009, MNRAS, 397, L82
Watson C. A., Dhillon V. S., Rutten R. G. M., Schwope A. D., 2003, MNRAS, 341, 129
Zorotovic M., Schreiber M. R., Gänsicke B. T., 2011, A&A, 536, A42

This paper has been typeset from a TeX/LaTeX file prepared by the author.